The impact of marine nutrient abundance on early eukaryotic ecosystems

[1,2]Christopher T. Reinhard, [2,3]Noah J. Planavsky, [4]Ben A. Ward, [2,5]Gordon D. Love, [6]Guillaume Le Hir, [2,5]Andy Ridgwell

[1]School of Earth and Atmospheric Sciences, Georgia Institute of Technology, Atlanta, GA 30332
[2]NASA Astrobiology Institute, Alternative Earths Team, Riverside, CA
[3]Department of Geology and Geophysics, Yale University, New Haven, CT 06511 [4]Ocean and Earth Science, University of Southampton, UK
[5]Department of Earth Sciences, University of California, Riverside, CA, USA
[6]Institute de Physique du Globe de Paris, Paris, FR
[7]School of Geographical Sciences, University of Bristol, Bristol, UK

ABSTRACT

The rise of eukaryotes to ecological prominence represents one of the most dramatic shifts in the history of Earth's biosphere. However, there is an enigmatic temporal lag between the emergence of eukaryotic organisms in the fossil record and their much later ecological expansion. In parallel, there is evidence for a secular increase in the availability of the key macronutrient phosphorus (P) in Earth's oceans. Here, we use an Earth system model equipped with a size-structured marine ecosystem to explore relationships between plankton size, trophic complexity, and the availability of marine nutrients. We find a strong dependence of planktonic ecosystem structure on ocean nutrient abundance, with a larger ocean nutrient inventory leading to greater overall biomass, broader size spectra, and increasing abundance of large zooplankton. If existing estimates of Proterozoic marine nutrient levels are correct, our results suggest that increases in the ecological impact of eukaryotic algae and trophic complexity in eukaryotic ecosystems were directly linked to restructuring of the global P cycle associated with the protracted rise of surface oxygen levels. Our results thus suggest an indirect but potentially important mechanism by which ocean oxygenation may have acted to shape marine ecological function during late Proterozoic time.

1. Introduction

The first-order features of Earth's biosphere have undergone fundamental transformations over time. In particular, the structure and composition of surface ocean ecosystems and the metabolic and taxonomic affinities of dominant primary producers have changed dramatically. Initial primary producing communities on Earth would have been composed entirely of anoxygenic photosynthetic bacteria (Xiong et al., 2000; Olson, 2006), and for much of Earth's subsequent history cyanobacteria are thought to have been the principal oxygenic photosynthesizer (Falkowski

et al., 2004; Johnston et al., 2009; Knoll, 2014). Eukaryotes are generally thought to have evolved relatively early—almost 2,000 million years ago (Ma) (Knoll, 2014). The oldest likely eukaryotic microfossils occur in the latest Paleoproterozoic Changzhougou (~1,800 Ma) and Chuanlinggou (~1,700 Ma) Formations of North China (Lamb et al., 2009; Peng et al., 2009). The oldest definitive eukaryotic microfossils—forms such as Shuiyousphaeridium, Tappania, Satka, and Valeria, characterized by morphological complexity, large size, and encystment structures—occur in the latest Paleoproterozoic-early Mesoproterozoic (~1,800-1,600 Ma) Ruyang Group of China (Pang et al., 2015) and the Mesoproterozoic (~1,500 Ma) Roper Group of Australia (Javaux et al., 2004).

However, eukaryotic organisms do not become a key component of surface ocean ecosystems until much later in Earth's history (Fig. 1), with no evidence of an important role for eukaryotic algae in primary production or of significant trophic structure in eukaryotic ecosystems emerging until after ~800 Ma (Knoll, 2014; Brocks et al., 2016). The oldest sterane biomarkers, recovered from kerogen and bitumen extracted from Tonian and Cryogenian strata, record the initiation of a measurable eukaryotic contribution to primary production during this same interval (Brocks et al., 2016; Brocks et al., 2017; Zumberge et al., In press). Although it is possible that some of the earliest eukaryotic fossils are from stem groups that did not produce sterols (Porter et al., 2018), the nearly billion-year gap between the Mesoproterozoic emergence of bona fide eukaryotic microfossils and the appearance of eukaryote-produced steranes in the Neoproterozoic is typically linked to environmental inhibition of eukaryotes through most of Proterozoic time (Brocks et al., 2017).

As a backdrop to this ecological and evolutionary history, marine surface environments have also evolved considerably over time. The abundance of oxygen (O_2) in Earth's ocean-atmosphere system has steadily and significantly increased through Earth's history (Holland, 1984; Kump, 2008; Lyons et al., 2014). In addition, there is complementary evidence from the rock record and biogeochemical models that the inventory of dissolved phosphorus (P) in Earth's oceans has increased throughout Earth's history (Fig. 1), broadly in step with the protracted oxygenation of the ocean-atmosphere system (Lenton and Watson, 2004; Papineau, 2010; Planavsky et al., 2010; Laakso and Schrag, 2014,2017; Reinhard et al., 2017; Ozaki et al., 2019). Existing empirical records suggest that global rates of primary productivity (and by inference marine nutrient levels)

during some periods of the mid-Proterozoic (~1.8-0.8 billion years ago, Ga) were likely less than ~10% of the modern Earth (Crockford et al., 2018), which is also consistent with global biogeochemical models of the coupled carbon and oxygen cycles for this time interval (Derry, 2015; Laakso and Schrag, 2018; Ozaki et al., 2019).

In theory, a link should exist between increases in marine P inventories and significant shifts in ecosystem structure. Both low-order idealized treatments (e.g., Armstrong, 1994,1999) and large-scale mechanistic models (e.g., Ward et al., 2012; Ward et al., 2014) predict that the availability of nutrients plays an important 'bottom-up' role in controlling marine ecosystem structure and trophic complexity. Specifically, the basic features of modern plankton biogeography and size spectra can be reproduced reasonably well in theoretical models by assuming only that small phytoplankton cells have high nutrient affinities and are capable of rapid growth and that population-level rates of mortality in phytoplankton are density-dependent. Several important predictions for surface ocean ecosystems emerge from these principles. When considering only growth and nutrient utilization, smaller (e.g., cyanobacterial) cells should outcompete larger (e.g., photosynthetic eukaryotic, or algal) cells essentially everywhere, because their smaller sizes correspond to higher growth rates and greater affinity for limiting nutrients (though exceptions to this might occur in highly perturbed/seasonal environments). Algal abundance in modern oceans is therefore generally linked to a 'top-down' (grazing) control on the abundance of smaller cells—which acts to prevent smaller primary producers from sequestering all of a limiting resource—while total biomass within the system is controlled by nutrient supply (Price et al., 1994; Ward et al., 2014; Knoll and Follows, 2016). As a result, increasing nutrient supply can balance grazing pressure at progressively larger phytoplankton size classes, resulting in a broader size spectrum, greater scope for the population of higher trophic levels, and greater overall biomass in the ecosystem. Conversely, severely nutrient-limited systems should come to be dominated by small phytoplankton cells, with little overall biomass and limited scope for the development of predation and higher trophic structure.

Here, we use a size-structured marine ecosystem model, embedded in an Earth system model of intermediate complexity (cGENIE) and configured for an illustrative interval of late Proterozoic time, to explore the impact of marine nutrient abundance on trophic structure and algal cell size. We find that the chronic P limitation characteristic of most of Earth's history (Bjerrum and

Canfield, 2002; Laakso and Schrag, 2014; Derry, 2015; Jones et al., 2015; Planavsky, 2015; Laakso and Schrag, 2017; Reinhard et al., 2017; Laakso and Schrag, 2018; Ozaki et al., 2019) would have yielded generally small phytoplankton cell size, limiting the trophic scope of early eukaryotic ecosystems in surface ocean environments and attenuating production and export of biomass from the photic zone. Building on this framework, we suggest that the temporal correspondence between a significant shift in the Earth surface P cycle (Planavsky et al., 2010; Reinhard et al., 2017), the expansion of eukaryotic algae (Cohen and Macdonald, 2015; Brocks et al., 2017; Gueneli et al., 2018; Isson et al., 2018), and increasing evidence of predation in surface ocean ecosystems (Porter et al., 2003; Porter, 2016) after nearly 1 billion years of apparent ecological stasis (Knoll, 2014) may have been a natural outcome of an increase in marine nutrient supply linked to the long-term oxygenation of Earth's ocean-atmosphere system.

2. Model Description

2.1. The cGENIE Earth system model

We employ a carbon-centric version of the Grid ENabled Integrated Earth system model (cGENIE), an Earth system model of intermediate complexity (EMIC) previously used to explore links between climate and ocean biogeochemistry on a range of timescales (Ridgwell, 2007; Meyer et al., 2008; Panchuk et al., 2008; Ridgwell and Schmidt, 2010; Cui et al., 2011; Monteiro et al., 2012; Gibbs et al., 2016; Kirtland Turner and Ridgwell, 2016; Olson et al., 2016; Reinhard et al., 2016; Gutjahr et al., 2017). The ocean physics and climate model in cGENIE is comprised of a reduced physics (frictional geostrophic) 3-D ocean circulation model, coupled to a 2-D energy-moisture balance model (EMBM) and a dynamic-thermodynamic sea ice model. The ocean transports heat, salinity, and a suite of biogeochemical tracers, exchanges heat and moisture with the atmosphere, sea ice, and land, and is forced at the ocean surface by the input of zonal and meridional wind stress by an imposed wind field. The EMBM considers heat and moisture balance within the atmospheric boundary layer, with air temperature and specific humidity as prognostic tracers. Moisture and heat are mixed horizontally throughout the 2-D atmosphere, and are exchanged with the ocean and land surface with precipitation occurring above a prescribed threshold in relative humidity. The sea ice model tracks the horizontal transport of sea ice, and the exchange of heat and freshwater with the ocean and atmosphere using ice thickness, areal fraction,

and concentration as prognostic variables. Full descriptions of the model and coupling procedure can be found in Edwards and Marsh (2005) and Marsh et al. (2011).

The biogeochemical model regulates air-sea gas exchange and the partitioning and transformation of biogeochemical tracers and isotopes within the ocean and atmosphere. By default, the ocean biological pump is driven by an 'implicit' scheme in which a parameterized uptake of nutrients occurs in the surface ocean, followed by stoichiometric conversion to dissolved or particulate organic matter for downstream transport, sinking, and remineralization (Ridgwell et al., 2007). Dissolved organic matter is transported by the ocean model and decays with a prescribed time constant, while particulate organic matter is immediately exported out of the surface ocean and is partitioned into two fractions of differing lability. In the ocean interior, particulate organic matter is remineralized instantaneously throughout the water column following an exponential decay function with a specified remineralization length scale for each fraction. The biological pump and inorganic carbon cycle within cGENIE, as well as the approach toward parameter calibration through data assimilation of modern tracer climatology, are described in detail in Ridgwell et al. (2007).

2.2. EcoGEnIE: A size-structured ecological model

We replace the default implicit scheme of stoichiometric conversion of nutrients to organic matter in the surface ocean within cGENIE with a recently developed ecological model that explicitly resolves a size-structured plankton community—EcoGEnIE (Ward et al., 2018). The EcoGEnIE model distinguishes a prescribed number of plankton populations (Fig. 2) that are defined based on their trophic functionality (e.g., phytoplankton, zooplankton, mixotroph) and organism size (equivalent spherical diameter, ESD). These features then regulate the ecophysiological traits of each plankton group, such as rates of growth (e.g., nutrient uptake), grazing, and mortality. Phytoplankton growth and nutrient uptake are co-limited by nutrient availability, light, and temperature, where both the maximum rate of nutrient uptake and overall nutrient affinity are dependent on the phytoplankton size (Moloney and Field, 1989,1991; Armstrong, 1994,1999; Ward et al., 2012; Ward et al., 2014) and functional group.

Zooplankton predation (grazing) scales with temperature and the abundance of potential prey biomass, and is constrained by a maximum grazing rate that is size-dependent (here we use

'zooplankton' to mean all plankton engaging in heterotrophy). The availability of potential prey is described as a roughly log-normal function of the predator-to-prey length ratio, with zooplankton predominantly grazing on prey that are ~10 times smaller (Fig. 2). Predators may also engage in 'active switching' (Kiørboe et al., 1996; Kiørboe, 2011; Vallina et al., 2014), preferentially grazing on prey that are relatively more available. Prey is assimilated into predator biomass with an efficiency for each element that is based on the respective predator quota for that element, leading to some fraction of prey biomass that is lost to the organic matter pool as a result of 'messy feeding' (Hygum et al., 1997; Møller, 2005). All living biomass is subject to a linear mortality rate, with plankton mortality reduced at biomass levels below ~10^{-6} mmolC m^{-3} such that a viable population is maintained within every surface grid cell of the ocean model (Ward et al., 2018). This biomass level is sufficiently small it does not significantly impact other components of the ecosystem or the abundance and transformation of biogeochemical tracers.

The basic approach is to initialize the model with dissolved phosphate (PO_4^{3-}) inventories ranging from 1% to 200% of the present oceanic level (POL; e.g., 1 POL represents a mean PO_4^{3-} inventory of 2.16 μmol kg^{-1}) and spin the model up to steady state for 10,000 years, allowing 3-D nutrient distributions within the ocean to come into equilibrium with the background climate state and marine plankton ecology. Our default ecosystem configuration – referred to here as the '2-guild' model (Table 1) – includes a total of 16 plankton size classes, with 8 size classes each of phytoplankton and zooplankton covering a size range between 200 nm and 1.9 mm (equivalent spherical diameter; ESD), similar to that explored in Ward et al. (2018). In this configuration, phytoplankton and zooplankton are strictly autotrophic or heterotrophic, respectively. We also evaluate an ensemble using a 'mixotroph' configuration in which the same size range as our default ensemble is spread across 9 mixotrophic size classes, which can use light and inorganic nutrients autotrophically and also ingest prey (Table 2). This strategy is common in the modern ocean (Sanders, 1991; Jones, 2000; Hartmann et al., 2012; Ward and Follows, 2016; Stoecker et al., 2017) and has been shown to have potentially significant impacts on carbon, nutrient, and energy fluxes through marine and freshwater ecosystems (Tittel et al., 2003; Ward and Follows, 2016). Lastly, we evaluate an ensemble with 64 total plankton size classes ('n64), distributed evenly between 32 phytoplankton and 32 zooplankton (Table 3), in order to examine the impact of a less 'quantized' size distribution.

2.3. Late Cryogenian configuration of cGENIE

Because our main goal is to explore the factors leading to the rise in abundance of larger eukaryotic organisms in marine ecosystems, we employ a roughly late Cryogenian configuration of cGENIE. The ocean bathymetry and land-sea mask are derived from the 635 Ma configuration of Goddéris et al. (2017). Solar luminosity is calculated according to Gough (1981) (see also Feulner, 2012), and is set to 1295.97 W m^{-2} (i.e., a reduction of 5.3% relative to the modern value of 1368 W m^{-2}). In our 'default' ensemble atmospheric pCO_2 remains fixed at 3,336 ppm (~12 times the present atmospheric level, PAL), with surface wind fields that are derived offline from GCM simulations (Fig. 3A). Similarly, we take a zonal mean planetary albedo profile directly from the coupled GCM simulations run at 3,336 ppm and apply it to cGENIE. We also explored the possible impact of background climate state by running two additional variable nutrient ensembles with the default (2-guild) plankton configuration. First, we perform a series of simulations with an elevated atmospheric pCO_2 of 20 PAL, sufficient to significantly increase sea surface temperatures both locally (Fig. 3G-I) and in the global average (with mean sea surface temperature (SST) increasing from 18.9ºC to 20.8ºC). We then perform the same set of simulations at a reduced atmospheric pCO_2 of 3 PAL, sufficient to significantly decrease mean SST from 18.9ºC to 14.3ºC, expand austral sea ice coverage, and nucleate boreal sea ice, but without initiating a 'snowball Earth' glaciation (Fig. 3D-F).

The ocean model in all simulations is configured as a 36 x 36 equal-area grid (uniform in longitude and uniform in the sine of latitude) with 16 logarithmically-spaced depth levels and seasonal surface forcing from the EMBM. Mean ocean salinity in the model is initialized at 33.9 PSU (~1 PSU lower than modern), consistent with an ice-free climate state at ~635 Ma. All simulations assume a fixed atmospheric pO_2 of 10% PAL, and an initial ocean dissolved sulfate (SO_4^{2-}) inventory of 1 mmol kg^{-1}. In the absence of good alternative constraints, the mean Mg/Ca ratio of the ocean is maintained at the modern value (10.28 mmol kg^{-1} Ca^{2+} and 52.82 mmol kg^{-1} Mg^{2+}). Ocean biogeochemistry is initialized with a homogeneous distribution of tracers and plankton biomass, and the model is spun up for 10,000 years to ensure attainment of steady state. All model results shown here are annual averages from the last model year. The model code plus all configuration files and parameter values needed to run the simulations reported here are provided together with full instructions on GitHub (see *Code Availability*).

3. Results

We find that changes in the marine phosphate inventory have a significant impact on the distribution of different plankton size classes in the surface ocean in our 2-guild model of the Proterozoic Earth (Fig. 4). At an ocean nutrient inventory characteristic of the modern Earth (Fig. 4G-I) smaller phytoplankton size classes (picophytoplankton, ≤2μm in diameter, and nanophytoplankton, 2-20μm in diameter) are present at significant biomass throughout the global surface ocean, while the largest phytoplankton size classes (microphytoplankton, >20μm in diameter) remain restricted to higher latitudes. This distribution is essentially that of the contemporary surface ocean. In contrast, at a global ocean nutrient inventory equivalent to 10% POL (Fig. 4D-F) picophytoplankton tend to be evenly distributed globally, with populations of nannophytoplankton abundant only at high latitudes and with microphytoplankton biomass essentially negligible on a global scale. Further decreasing the ocean nutrient inventory to 1% POL results in negligible biomass within both nanophytoplankton and microphytoplankton size classes, and restricts picophytoplankton to high latitudes where vertical exchange with deep ocean nutrients is enhanced (Fig. 4A-C). These changes in distribution are accompanied by significant decreases in mean and maximum phytoplankton cell size and a dramatic drop in the overall size of Earth's autotrophic biosphere (Fig. 5).

The results of our ensemble of Earth system/marine ecosystem model simulations suggest that as ocean nutrient inventories increase, the expansion of biomass into progressively larger size classes (and, implicitly, an expansion of the importance of eukaryotic phytoplankton relative to photosynthetic bacteria) has dramatic effects on the trophic scope of surface ocean ecosystems. To illustrate this, we analyze the abundance and distribution of the 190 μm zooplankton size class (and the same mixotrophic size class in our 'mixotroph-only' model), using this as a trophic proxy for early eukaryotic predators such as relatively small planktonic rhizarians and other ecologically similar eukaryotic micropredators (Andersen et al., 2016; Porter, 2016). We do not mean to suggest that a given size class corresponds precisely to any particular clade, or that substantial eukaryotic trophic complexity cannot exist within smaller size classes (i.e., picoeukaryotes; Massana, 2011). Nevertheless, we consider this portion of the size spectrum to be a reasonable ecological 'proxy' for the appearance of relatively large eukaryotic predators in the fossil record (Porter and Knoll, 2000; Porter, 2016).

We find that the distribution of the 190 μm size class is severely restricted below nutrient levels of ~10% those of the modern Earth for both our 2-guild and mixotroph-only models (Fig. 6A-D). We also find that for any given ocean nutrient inventory mixotrophy enhances the transfer of nutrients and biomass through planktonic ecosystems, supporting relatively greater biomass in larger size classes at a given set of conditions relative to the 2-guild model (Fig. 6). This is consistent with previous work exploring the potential role of mixotrophy in amplifying carbon and energy fluxes through modern marine ecosystems (Ward and Follows, 2016). However, the overall magnitude of this difference decreases sharply at progressively lower ocean nutrient inventories, and even entirely mixotrophic biospheres show limited capacity to support large eukaryotic predator biomass at estimated Proterozoic nutrient inventories (Fig. 6, 7).

In order to estimate the impact of marine nutrient inventory on the abundance of large predatory eukaryotes on a global scale, we calculate the total integrated plankton biomass present in the 190 μm size class for the default ('2-guild'), mixotroph-only ('mixo'), and 64-size-class ('n64') configurations, and compare this with available estimates for ocean nutrient levels during Proterozoic time (Fig. 7). Overall biomass (and thus implicitly the scope for large eukaryotic predators) are severely curtailed in our models at estimated Proterozoic ocean nutrient levels based on the geochemistry of iron-rich marine sedimentary rocks (Jones et al., 2015) and large-scale biogeochemical models (Laakso and Schrag, 2017; Reinhard et al., 2017; Ozaki et al., 2019). Trophic transfer to predatory size classes is enhanced in the mixotroph-only model, but our model predicts that the effect of this on a global scale would have been very small at estimated ocean nutrient levels during the Proterozoic. There is a coherent, though relatively small, increase in zooplankton predator biomass atmospheric pCO_2 drops, which we attribute to decreased nutrient utilization at colder temperatures with more extensive sea ice coverage near the poles. However, the effect is small, with all ensembles showing the same sharp increase in globally integrated zooplankton predator biomass at oceanic nutrient inventories significantly above ~10% that of the modern Earth (Fig. 7).

4. Discussion

Our model results suggest that changes in the ocean nutrient inventory during Proterozoic time may have exerted significant leverage over marine trophic structure and the evolutionary ecology

of early eukaryotes. However, a number of interesting issues remain to be explored in similar models and grounded in observations from the geologic record. For example, we do not explicitly link the strength of the biological pump to phytoplankton cell size, and we anticipate that expansion of the plankton size structure will feed back into ocean redox structure and surface nutrient availability on timescales of ~10^2 – 10^4 years. These changes would be further modulated by shifts in the biomass C/P ratio of primary producers driven by changes to nutrient availability and trophic structure (Deutsch and Weber, 2012; Reinhard et al., 2017; Moreno and Martiny, 2018), all of which will feed back into the global carbon and oxygen cycles on timescales that scale to some extent with atmospheric pO_2 but approach ~10^6 years when atmospheric pO_2 is relatively high (Holland, 1984). Finally, while our model results provide persuasive evidence for the centrality of marine P levels in controlling ecosystem structure, they are incapable of constraining the mechanistic drivers that may have led to significant shifts in P cycling during the late Proterozoic.

Nevertheless, our model results provide a simple explanation for the macroevolutionary lag between the initial appearance of total- and crown-group eukaryotes in the microfossil record (Javaux et al., 2001,2004; Knoll et al., 2006; Lamb et al., 2009), and as predicted from molecular clocks (Parfrey et al., 2011; Betts et al., 2018), and the much later expansion of eukaryotic algae, micropredators, and more complex heterotrophs observed in the molecular biomarker, microfossil, genomic, and geochemical records (Porter and Knoll, 2000; Porter et al., 2003; Love et al., 2009; Knoll, 2014; Cohen and Macdonald, 2015; Gold et al., 2016; Porter, 2016; Gueneli et al., 2018; Isson et al., 2018; Zumberge et al., 2018; van Maldegem et al., 2019; Zumberge et al., In press). In addition, these results provide persuasive additional evidence for a straightforward mechanistic link between changes to ocean nutrient levels and the "rise of algae" during late Proterozoic time (Brocks et al., 2017; Zumberge et al., In press), in which increasing availability of P to surface marine ecosystems allowed for an expansion in the size spectra of autotrophs and increased trophic scope among larger eukaryotic predators (including sponge-grade metazoans; Love et al., 2009; Zumberge et al., 2018). This style of trophic escalation, driven by increasing nutrient availability, has been previously invoked to explain changes to molecular biomarker assemblages and stable isotope compositions (Brocks et al., 2017; Gueneli et al., 2018) and turnover of eukaryotic acritarch lineages during the late Proterozoic (Knoll, 1994; Vidal and Moczydlowska-Vidal,

1997). Our results support this, and provide a series of spatially explicit predictions that can be further tested against more detailed paleontological and geochemical records.

Our results also provide a new perspective on the potential mechanistic links between ocean-atmosphere oxygenation on Earth and the ecological expansion of animal life, as they suggest that a relatively large ocean nutrient inventory is a prerequisite for the upstream ecological expansion of larger, more complex organisms in benthic habitats. Indeed, limited carbon delivery to the benthic realm may have been a central ingredient in the confluence of ecological factors constraining early metazoan communities (Sperling and Stockey, 2018). Low nutrient levels are in turn thought to be strongly impacted by surface oxygen levels and the marine redox landscape (Laakso and Schrag, 2014; Derry, 2015; Jones et al., 2015; Reinhard et al., 2017), providing a direct but previously unrecognized mechanistic link between ocean-atmosphere O_2 abundance and the evolutionary ecology of early animal life. In particular, the levels of ocean-atmosphere O_2 required to support large ocean nutrient inventories may be significantly different from those required for the resting and/or active metabolisms of basal aerobic metazoans. Indeed, the estimated O_2 requirements of early animals are potentially very low (Sperling et al., 2013; Mills et al., 2014), while the atmospheric O_2 levels required to maintain large ocean nutrient inventories may be considerably higher (Laakso and Schrag, 2014; Reinhard et al., 2017). Fully constraining the offset between these two surface O_2 levels and their potential impacts on ocean chemistry and evolution remains an important task for future work. In any case, our results suggest that the sharp rise in eukaryotic diversification and the complexity of surface ocean ecosystems during the late Proterozoic may have been mechanistically linked to changes in ocean redox structure, nutrient availability, and atmospheric O_2 abundance.

5. Conclusions

If existing estimates of Proterozoic marine nutrient levels are correct, our model results indicate that shifts in Earth's phosphorus cycle during late Proterozoic time would have resulted in dramatic changes in the scope for upward energy flow and eukaryotic predation in ocean ecosystems. These shifts would be predicted to have significant downstream impacts on carbon and energy fluxes to the benthic realm, linking marine nutrient abundance to the ecology of early animal life. Our results also imply a novel, though indirect, link between the abundance of O_2 in Earth's atmosphere and

the trophic scope of marine ecosystems, through the relationships that link ocean-atmosphere O_2 and Earth's phosphorus cycle on geologic timescales. When considered in light of progressively more quantitatively precise and stratigraphically continuous empirical constraints on marine nutrient abundance and ocean-atmosphere oxygenation, spatially explicit modeling of planktonic ecosystems has the potential to provide important insight into the environmental context for the emergence and expansion of biological complexity on the late Proterozoic Earth.

6. Code Availability

A manual describing code installation, basic model configuration, and an extensive series of tutorials is provided. The Latex source of the manual and PDF file can be obtained by cloning (https://github.com/derpycode/muffindoc). The user manual contains instructions for obtaining, installing, and testing the code, as well as running experiments. The version of the code used in this paper is tagged as release v0.9.9 and has a DOI of 10.5281/zenodo.3620841. Configuration files for the specific experiments presented in the paper can be found in: cgenie.muffin/genie-userconfigs/MS/reinhardetal.Geobiology.2020. Details of the different experiments, plus the command line needed to run each, are given in README.txt.

Acknowledgements. We are grateful to K. Konhauser for editorial handling. C.T.R. acknowledges the NASA Astrobiology Institute and the National Science Foundation for funding. B.A.W. is supported by a Royal Society University Research Fellowship. The development of the 'EcoGEnIE' ecosystem model was supported by EU grant ERC-2013-CoG-617303. A.R. was additionally supported in part by an award from the Heising-Simons Foundation.

TABLE AND FIGURE CAPTIONS:

Table 1. Plankton size distribution and functional designations for plankton classes for the default ('2-guild') ecosystem configuration. Sizes refer to the equivalent spherical diameter (ESD) of plankton cells.

j	*Functional Type*	ESD [μm]	*j*	*Functional Type*	ESD [μm]
1	phytoplankton	0.6	9	zooplankton	0.6
2	phytoplankton	1.9	10	zooplankton	1.9
3	phytoplankton	6.0	11	zooplankton	6.0
4	phytoplankton	19.0	12	zooplankton	19.0
5	phytoplankton	60.0	13	zooplankton	60.0
6	phytoplankton	190.0	14	zooplankton	190.0
7	phytoplankton	600.0	15	zooplankton	600.0
8	phytoplankton	1900.0	16	zooplankton	1900.0

Table 2. Plankton size distribution and functional designations for plankton classes for the mixotroph-only ('mixo') ecosystem configuration. Sizes refer to the equivalent spherical diameter (ESD) of plankton cells.

j	*Functional Type*	ESD [μm]
1	mixotroph	0.2
2	mixotroph	0.6
3	mixotroph	1.9
4	mixotroph	6.0
5	mixotroph	19.0
6	mixotroph	60.0
7	mixotroph	190.0
8	mixotroph	600.0
9	mixotroph	1900.0

Table 3. Plankton size distribution and functional designations for plankton classes in the 32x32 ('n64') ecosystem configuration. Sizes refer to the equivalent spherical diameter (ESD) of plankton cells.

j	*Functional Type*	ESD [μm]	*j*	*Functional Type*	ESD [μm]
1	phytoplankton	0.10	33	zooplankton	0.15
2	phytoplankton	0.15	34	zooplankton	0.20
3	phytoplankton	0.20	35	zooplankton	0.25
4	phytoplankton	0.25	36	zooplankton	0.30
5	phytoplankton	0.30	37	zooplankton	0.45
6	phytoplankton	0.45	38	zooplankton	0.60
7	phytoplankton	0.60	39	zooplankton	0.80
8	phytoplankton	0.80	40	zooplankton	1.10
9	phytoplankton	1.10	41	zooplankton	1.50
10	phytoplankton	1.50	42	zooplankton	2.00
11	phytoplankton	2.00	43	zooplankton	2.70
12	phytoplankton	2.70	44	zooplankton	3.60
13	phytoplankton	3.60	45	zooplankton	5.00
14	phytoplankton	5.00	46	zooplankton	6.70
15	phytoplankton	6.70	47	zooplankton	9.00
16	phytoplankton	9.00	48	zooplankton	12.20
17	phytoplankton	12.20	49	zooplankton	16.40
18	phytoplankton	16.40	50	zooplankton	22.20
19	phytoplankton	22.20	51	zooplankton	30.00
20	phytoplankton	30.00	52	zooplankton	40.40
21	phytoplankton	40.40	53	zooplankton	54.60
22	phytoplankton	54.60	54	zooplankton	74.00
23	phytoplankton	74.00	55	zooplankton	100.00
24	phytoplankton	100.00	56	zooplankton	134.00
25	phytoplankton	134.00	57	zooplankton	181.00
26	phytoplankton	181.00	58	zooplankton	244.70
27	phytoplankton	244.70	59	zooplankton	330.40
28	phytoplankton	330.40	60	zooplankton	446.00
29	phytoplankton	446.00	61	zooplankton	624.00
30	phytoplankton	624.00	62	zooplankton	874.20
31	phytoplankton	874.20	63	zooplankton	1224.00
32	phytoplankton	1224.00	64	zooplankton	2800.00

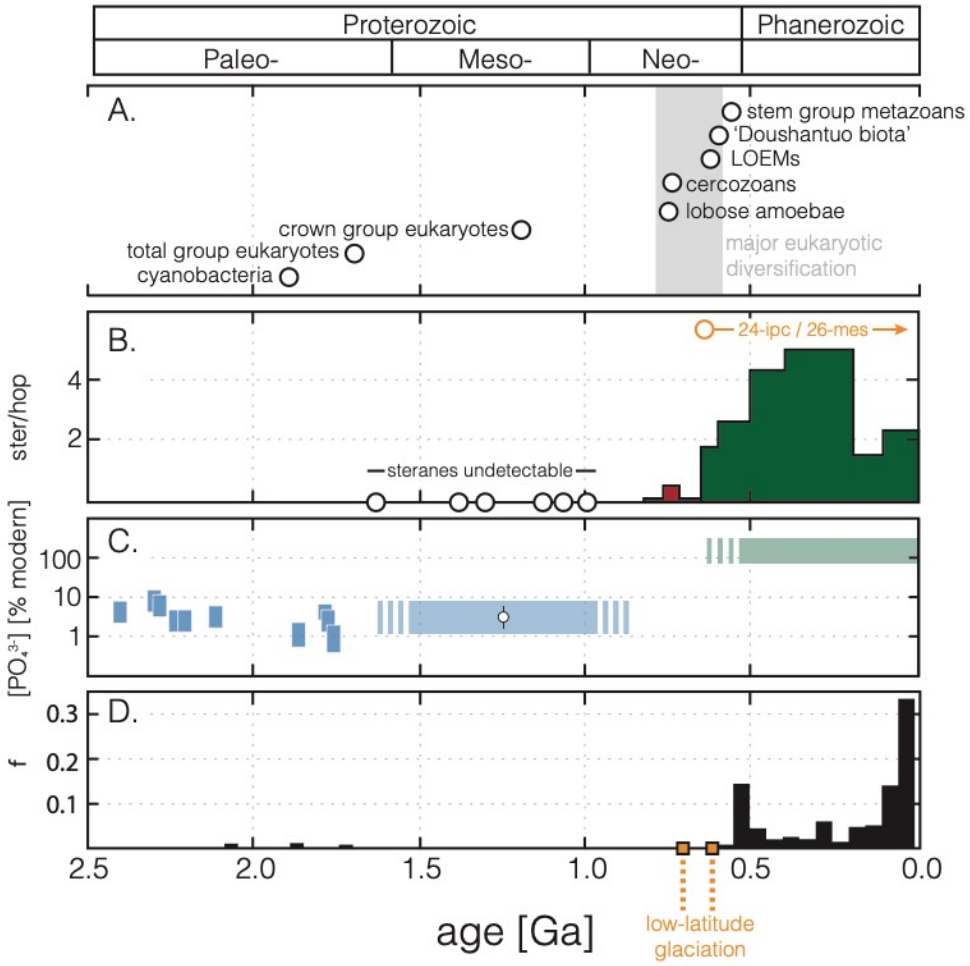

Figure 1. Summary of key late Proterozoic changes in the microfossil (**A**), molecular biomarker (**B**), and inorganic geochemical (**C, D**) records. (**A**) Approximate first appearance of major fossil groups and interval of major eukaryotic diversification summarized from (Hofmann, 1976; Butterfield, 2000; Porter et al., 2003; Xiao and Laflamme, 2008; Cohen et al., 2009; Knoll, 2011; Lyons et al., 2012; Knoll, 2014). (**B**) Maximum ratio of steranes (a molecular biomarker for eukaryotic algae) to hopanes (a molecular biomarker for bacteria) from organic geochemical records following (Brocks et al., 2017; Isson et al., 2018), where open circles denote undetectable sterane abundance. (**C**) Oceanic phosphate (PO_4^{3-}) abundance is depicted based on empirical constraints from Proterozoic iron-rich chemical sediments (filled blue squares; Jones et al., 2015); a stochastic inversion of mid-Proterozoic ocean chemistry based on a global marine biogeochemistry model (open circle and shaded blue field; Ozaki et al., 2019); and a time-dependent model of Phanerozoic ocean-atmosphere biogeochemistry (shaded green field; Lenton et al., 2018). Open circle, error bars, and shaded blue envelope in (**C**) denote the median, 1σ, and 95% credible intervals for the model inversion, while the shaded green envelope depicts the inclusive range of estimated deep ocean [PO_4^{3-}] values through the Phanerozoic. Shown in (**D**) is a summary of the relative abundance of large, stratigraphically continuous (thicker than ~5m) marine phosphorite deposits from the database given in (Planavsky, 2015).

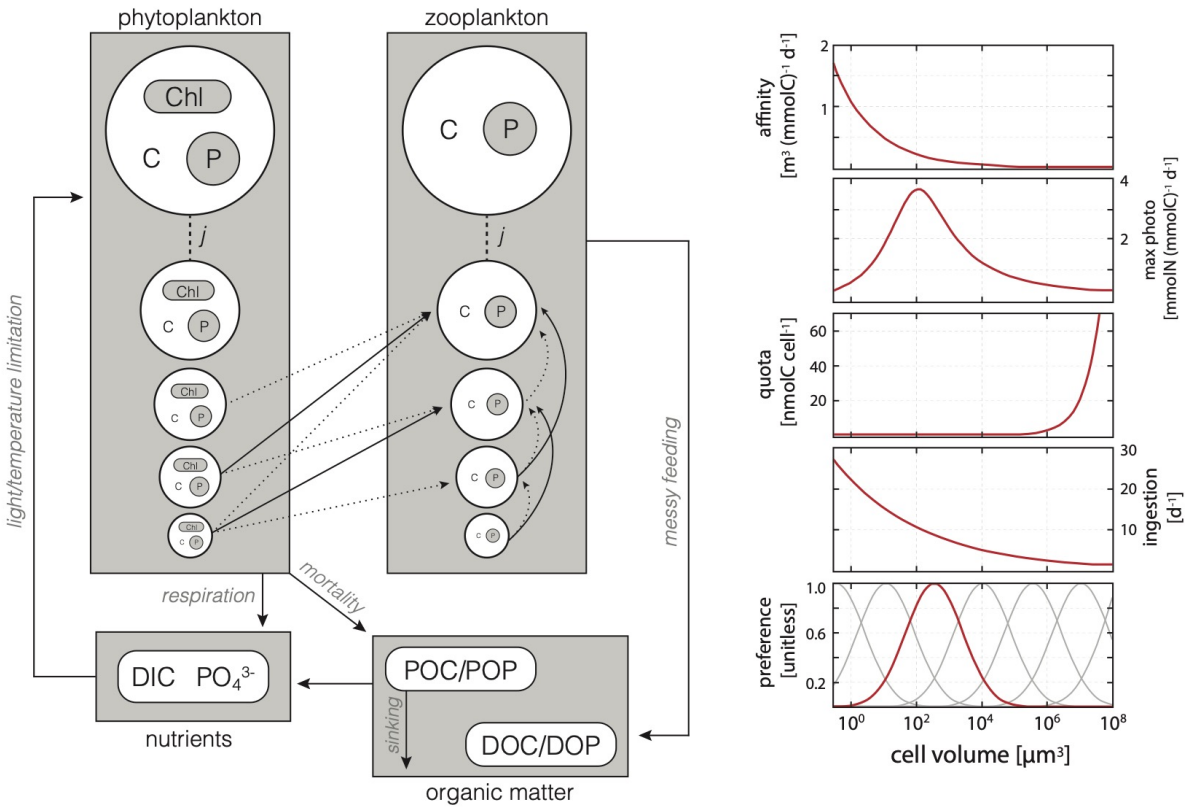

Figure 2. (Left) Schematic depiction of the size-structured plankton ecology model EcoGEnIE (Ward et al., 2018). The model resolves biomass-associated pools of chlorophyll (Chl), carbon (C), and phosphorus (P) in a prescribed number of plankton size classes, with zooplankton grazing on both phytoplankton and zooplankton in smaller size classes. Biomass-associated C and P can be remineralized directly to dissolved inorganic carbon (DIC) or dissolved phosphate (PO_4^{3-}), or can be transferred to the particulate/dissolved organic matter pool through cell mortality and messy feeding and subsequently remineralized to dissolved inorganic nutrients. (Right) Key size-dependent characteristics of the various plankton classes in EcoGEnIE, including (from top to bottom) autotrophic nutrient affinity and maximum rate of photosynthesis, per-cell carbon quota, zooplankton grazing rate, and the palatability of prey. For the latter, the preferred prey size range for a single zooplankton size class is shown in red, while those of other size classes are shown in grey. After Wilson et al. (2018).

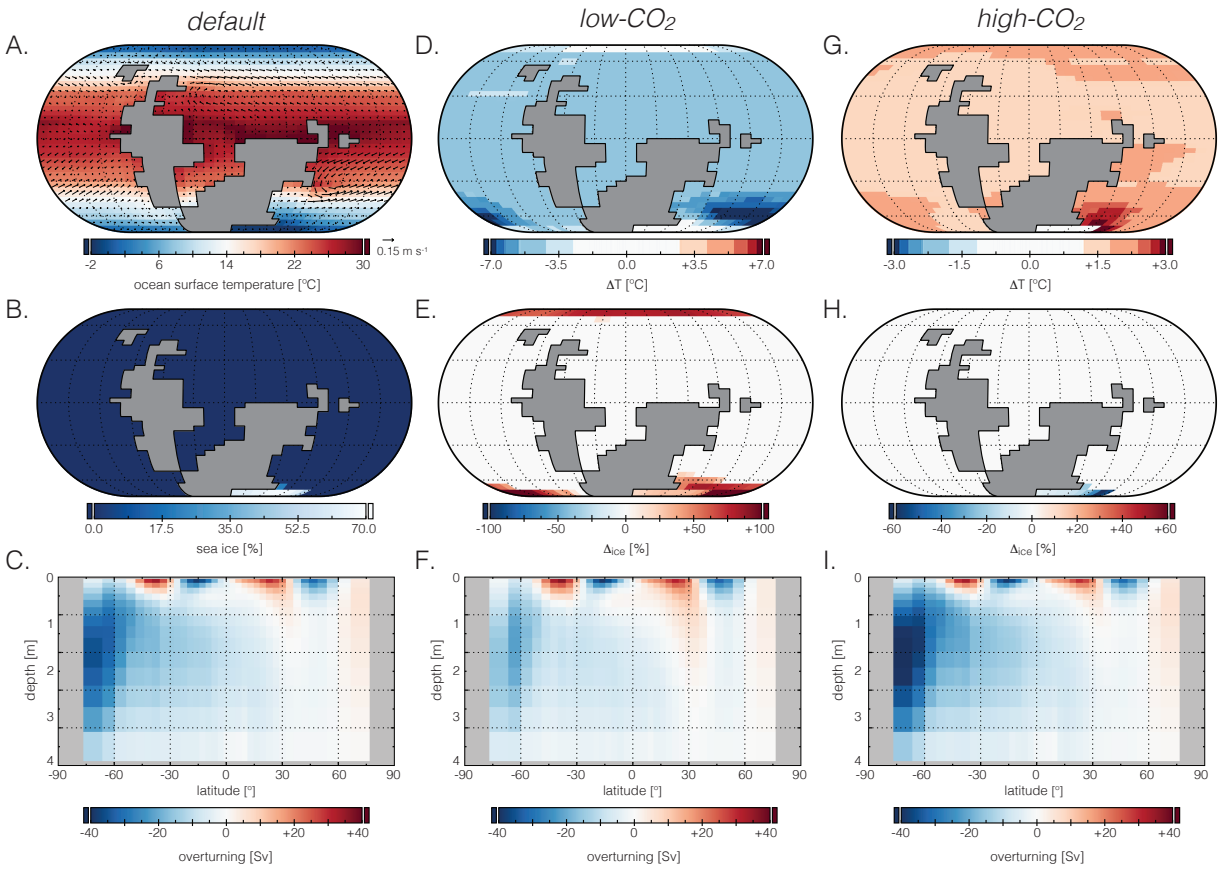

Figure 3. Ocean surface temperature, sea ice coverage, and global overturning circulation for our default (pCO_2 ~ 12PAL; **A-C**), low-CO_2 (pCO_2 ~ 3PAL; **D-F**), and high-CO_2 (pCO_2 ~ 20PAL; **G-I**) simulations. Ocean surface temperature (**A**) and sea ice cover (**B**) are both shown for the default case, while temperature and ice coverage anomalies are shown for the low-CO_2 (**D, E**) and high-CO_2 (**G, H**) cases. Also shown are surface ocean current speeds for the default climate state (**A**). Changes in ice coverage and ocean surface temperature lead to significant changes in deep ocean circulation, and in particular a notable strengthening (high CO_2) or weakening (low CO_2) of the strong circulation cell at southern high latitudes and a significant deepening of the shallower mid-latitude circulation cell at low CO_2 in the zonal average.

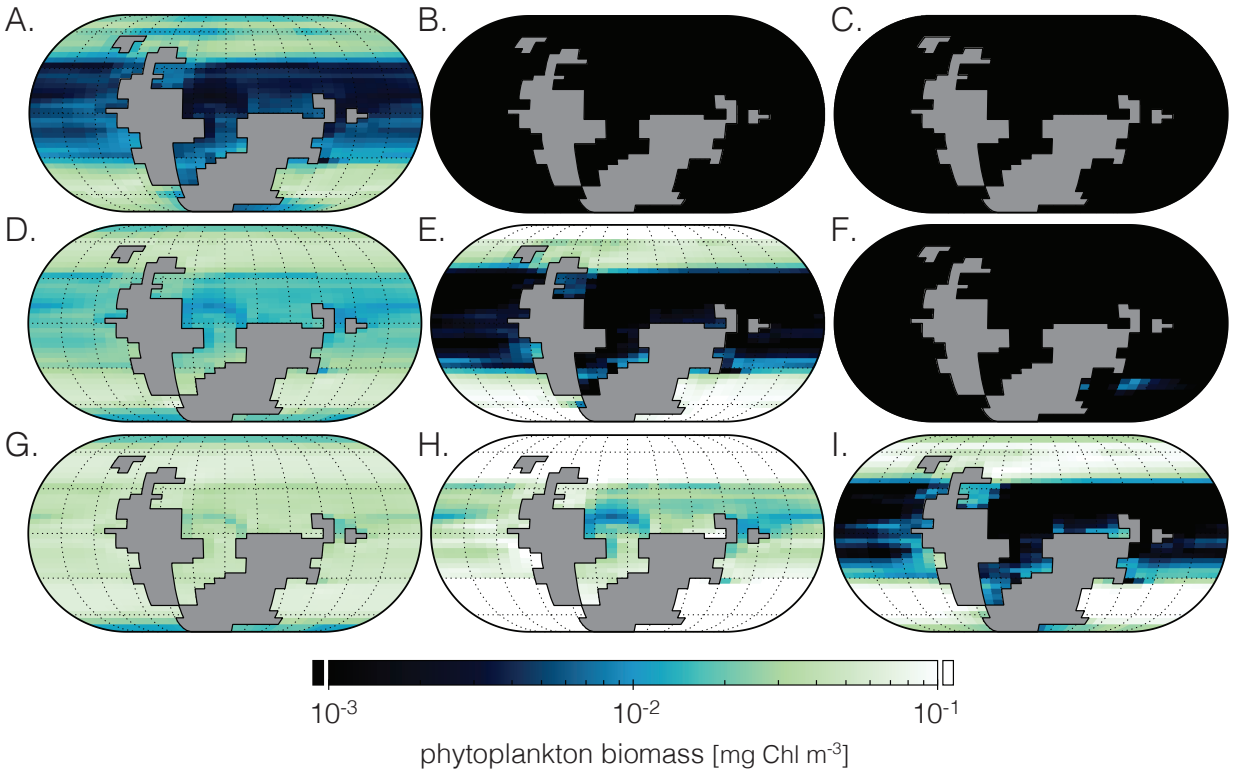

Figure 4. Steady-state phytoplankton biomass for major size classes of marine plankton under varying nutrient levels. Size classes include picophytoplankton (diameter ≤ 2µm; **A, D, G**), nanophytoplankton (diameter 2-20µm; **B, E, H**), and microphytoplankton (diameter > 20µm; **C, F, I**). Simulations were run at three different initial PO_4^{3-} inventories, 1% (**A-C**), 10% (**D-F**), and 100% (**G-I**) of the present oceanic level (POL). Note the log scale for biomass.

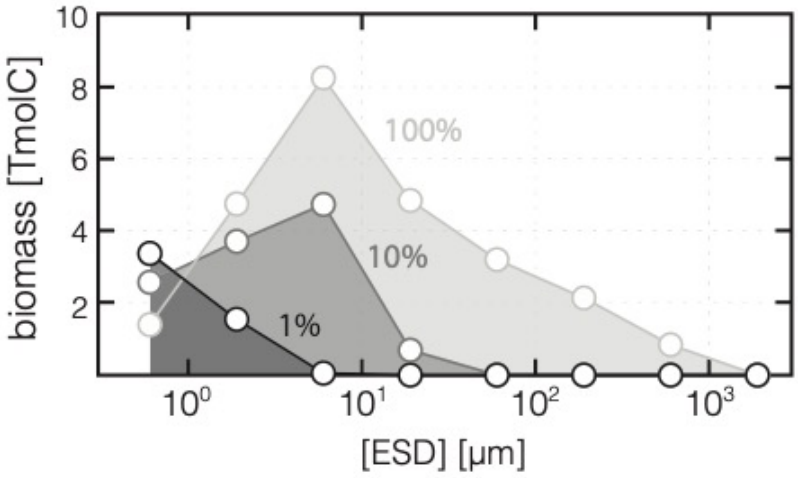

Figure 5. Phytoplankton size spectra as a function of marine nutrient inventory. Distributions show phytoplankton biomass as a function of size (in terms of equivalent spherical diameter, ESD) for marine nutrient levels of 1%, 10%, and 100% of the present oceanic level (POL). Increasing nutrient abundances are associated with significant broadening of phytoplankton size spectra, increased mean and maximum cell sizes, and greater overall sizes of the autotrophic biosphere.

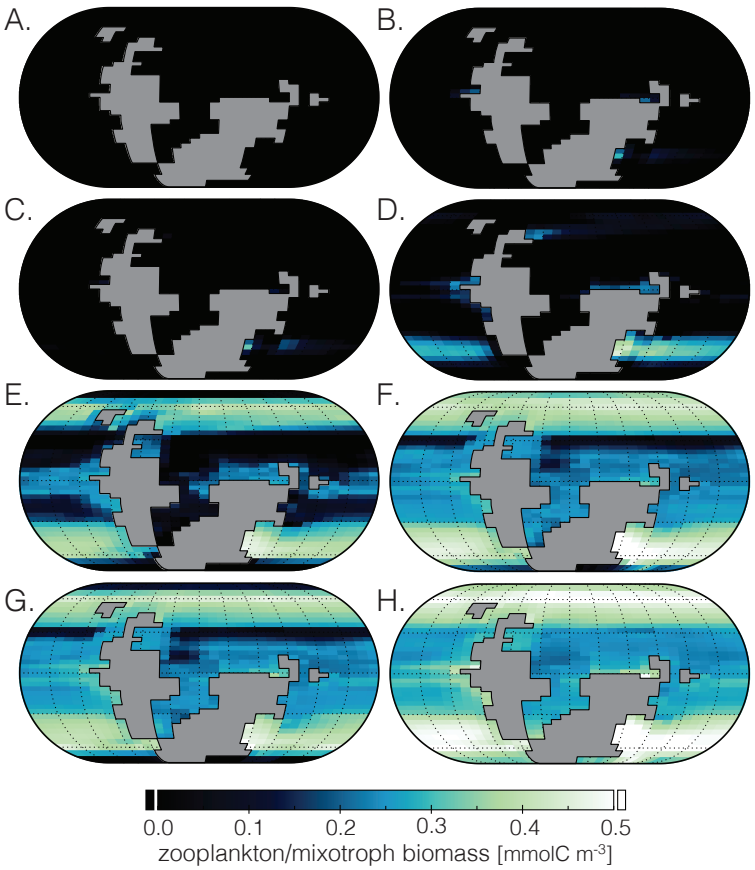

Figure 6. Nutrient controls on the distribution of large eukaryverous predators in late Proterozoic seas. Maps show surface standing biomass abundance in the 190 µm size class of zooplankton (for the 2-guild model; left) and mixotrophs (mixotroph-only model; right) at a range of marine nutrient levels. Rows correspond to simulations run at initial PO_4^{3-} inventories of 5% (**A, B**), 10% (**C, D**), 50% (**E, F**), and 100% (**G, H**) of the present oceanic level (POL).

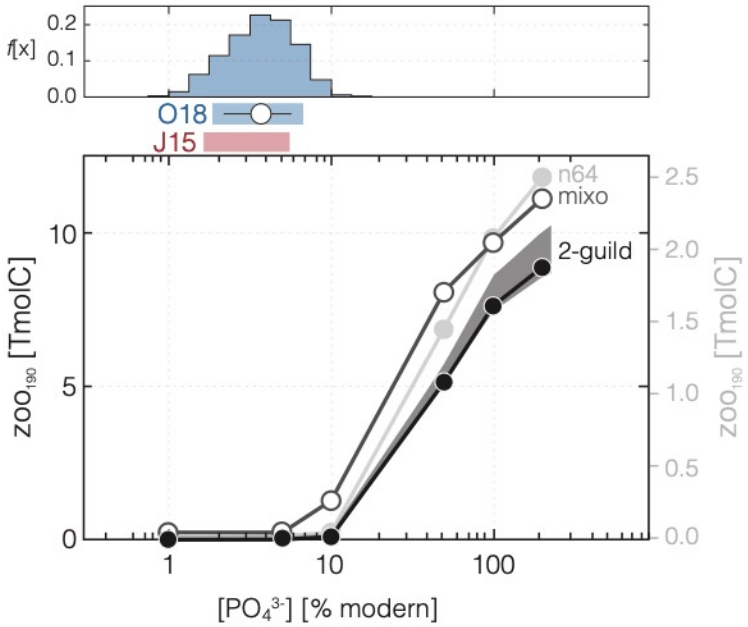

Figure 7. Integrated global biomass in the 190 μm plankton size class (P_{190}) for zooplankton ('2-guild', 'n64') and mixotrophs ('mixo') as a function of marine PO_4^{3-} inventory. Shown above are existing quantitative estimates for Proterozoic nutrient levels. The histogram in the upper panel depicts the posterior distribution for deep ocean dissolved PO_4^{3-} retrieved from a Monte Carlo inversion of an ocean biogeochemistry model, with the median (open circle), 1σ range (error bar), and 90% credible interval (shaded box) shown below (O18; Ozaki et al., 2019). This is compared with the range obtained from the P/Fe ratios of iron-rich marine chemical sediments assuming varying levels of dissolved Si, Ca^{2+}, and Mg^{2+} (J15; Jones et al., 2015). Note the differing scale for the n64 simulations, which plot to the right ordinate axis.

References:

Andersen KH, Berge T, Goncalves RJ, Hartvig M, Heuschele J, Hylander S, Jacobsen NS, Lindemann C, Matens EA, Neuheimer AB and others. (2016) Characteristic sizes of life in the oceans, from bacteria to whales. *Annual Review of Marine Science*, 8, 217-241.

Armstrong RA. (1994) Grazing limitation and nutrient limitation in marine ecosystems: Steady state solutions of an ecosystem model with multiple food chains. *Limnology and Oceanography*, 39, 597-608.

Armstrong RA. (1999) Stable model structures for representing biogeochemical diversity and size spectra in plankton communities. *Journal of Plankton Research*, 21, 445-464.

Betts HC, Puttick MN, Clark JW, Williams TA, Donoghue PCJ, and Pisani D. (2018) Integrated genomic and fossil evidence illuminates life's early evolution and eukaryote origin. *Nature Ecology & Evolution*, 2, 1556-1562.

Bjerrum CJ, and Canfield DE. (2002) Ocean productivity before about 1.9 Ga ago limited by phosphorus adsorption onto iron oxides. *Nature*, 417, 159-162.

Brocks JJ, Jarrett AJ, Sirantoine E, Hallmann C, Hoshino Y, and Liyanage T. (2017) The rise of algae in Cryogenian oceans and the emergence of animals. *Nature*, 548, 578-581.

Brocks JJ, Jarrett AJM, Sirantoine E, Kenig F, Moczydlowska M, Porter SM, and Hope J. (2016) Early sponges and toxic protists: possible sources of cryostane, an age diagnostic biomarker antedating Sturtian Snowball Earth. *Geobiology*, 14, 129-149.

Butterfield NJ. (2000) Bangiomorpha pubescens n. gen., n. sp.: implications for the evolution of sex, multicellularity, and the Mesoproterozoic/Neoproterozoic radiation of eukaryotes. *Paleobiology*, 26, 386-404. 10.1666/0094-8373(2000)026<0386:bpngns>2.0.co;2

Cohen PA, Knoll AH, and Kodner RB. (2009) Large spinose microfossils in Ediacaran rocks as resting stages of early animals. *Proceedings of the National Academy of Sciences, USA*, 106, 6519-6524.

Cohen PA, and Macdonald FA. (2015) The Proterozoic record of eukaryotes. *Paleobiology*. 10.1017/pab.2015.25

Crockford PW, Hayles JA, Bao H, Planavsky NJ, Bekker A, Fralick PW, Halverson GP, Bui TH, Peng Y, and Wing BA. (2018) Triple oxygen isotope evidence for limited mid-Proterozoic primary productivity. *Nature*, 559, 613-616.

Cui Y, Kump LR, Ridgwell A, Charles AJ, Junium CK, Diefendorf AF, Freeman KH, Urban NM, and Harding IC. (2011) Slow release of fossil carbon during the Palaeocene-Eocene Thermal Maximum. *Nature Geoscience*, 4, 481-485.

Derry LA. (2015) Causes and consequences of mid-Proterozoic anoxia. *Geophysical Research Letters*. 10.1002/2015GL065333

Deutsch C, and Weber T. (2012) Nutrient ratios as a tracer and driver of ocean biogeochemistry. *Annual Review of Marine Science*, 4, 113-141.

Edwards NR, and Marsh R. (2005) Uncertainties due to transport-parameter sensitivity in an efficient 3-D ocean-climate model. *Climate Dynamics*, 24, 415-433.

Falkowski PG, Katz ME, Knoll AH, Quigg A, Raven JA, Schofield O, and Taylor FJR. (2004) The evolution of modern eukaryotic phytoplankton. *Science*, 305, 354-360.

Feulner G. (2012) The faint youn Sun problem. *Reviews of Geophysics*, 50. 10.1029/2011RG000375

Gibbs SJ, Bown PR, Ridgwell A, Young J, Poulton AJ, and O'Dea SA. (2016) Ocean warming, not acidification, controlled coccolithophore response during past greenhouse climate change. *Geology*, 44, 59-62.

Goddéris Y, Le Hir G, Macouin M, Donnadieu Y, Hubert-Théou L, Dera G, Aretz M, Fluteau F, Li ZX, and Halverson GP. (2017) Paleogeographic forcing of the strontium isotopic cycle in the Neoproterozoic. *Gondwana Research*, 42, 151-162.

Gold DA, Grabenstatter J, de Mendoza A, Riesgo A, Ruiz-Trillo I, and Summons RE. (2016) Sterol and genomic analyses validate the sponge biomarker hypothesis. *Proceedings of the National Academy of Sciences, USA*, 113, 2684-2689.

Gough DO. (1981) Solar interior structure and luminosity variations. *Solar Physics*, 74, 21-34.

Gueneli N, McKenna AM, Ohkouchi N, Boreham CJ, Beghin J, Javaux EJ, and Brocks JJ. (2018) 1.1-billion-year-old porphyrins establish a marine ecosystem dominated by bacterial primary producers. *Proceedings of the National Academy of Sciences, USA*. 10.1073/pnas.1803866115

Gutjahr M, Ridgwell A, Sexton PF, Anagnostou E, Pearson PN, Pälike H, Norris RD, Thomas E, and Foster GL. (2017) Very large release of mostly volcanic carbon during the Palaeocene-Eocene Thermal Maximum. *Nature*, 548, 573-577.

Hartmann M, Grob C, Tarran GA, Martin AP, Burkill PH, Scanlan DJ, and Zubkov MV. (2012) Mixotrophic basis of Atlantic oligotrophic ecosystems. *Proceedings of the National Academy of Sciences, USA*, 109, 5756-5760.

Hofmann HJ. (1976) Precambrian microflora, Belcher Islands, Canada: Significance and systematics. *Journal of Paleontology*, 50, 1040-1073.

Holland HD. (1984) The Chemical Evolution of the Atmosphere and Ocean. Princeton University Press, Princeton, N.J.

Hygum BH, Petersen JW, and Søndergaard M. (1997) Dissolved organic carbon released by zooplankton grazing activity - a high-quality substrate pool for bacteria. *Journal of Plankton Research*, 19, 97-111.

Isson TT, Love GD, Dupont CL, Reinhard CT, Zumberge A, Asael D, Gueguen B, McCrow JP, Gill BC, Owens JD and others. (2018) Tracking the rise of eukaryotes to ecological dominance with zinc isotopes. *Geobiology*, 16, 341-352.

Javaux EJ, Knoll AH, and Walter MR. (2001) Morphological and ecological complexity in early eukaryotic ecosystems. *Nature*, 412, 66-69. 10.1038/35083562

Javaux EJ, Knoll AH, and Walter MR. (2004) TEM evidence for eukaryotic diversity in mid-Proterozoic oceans. *Geobiology*, 2, 121-132. 10.1111/j.1472-4677.2004.00027.x

Johnston DT, Wolfe-Simon F, Pearson A, and Knoll AH. (2009) Anoxygenic photosynthesis modulated Proterozoic oxygen and sustained Earth's middle age. *Proceedings of the National Academy of Sciences of the United States of America*, 106, 16925-16929. Doi 10.1073/Pnas.0909248106

Jones C, Nomosatryo S, Crowe SA, Bjerrum CJ, and Canfield DE. (2015) Iron oxides, divalent cations, silica, and the early earth phosphorus crisis. *Geology*, 43, 135-138.

Jones RI. (2000) Mixotrophy in planktonic protists: an overview. *Freshwater Biology*, 45, 219-226.

Kiørboe T. (2011) How zooplankton feed: mechanisms, traits and trade-offs. *Biological Reviews*, 86, 311-339.

Kiørboe T, Siaz E, and Viitasalo M. (1996) Prey switching behaviour in the planktonic copepod *Acartia tonsa*. *Marine Ecology Progress Series*, 143, 65-75.

Kirtland Turner S, and Ridgwell A. (2016) Development of a novel empirical framework for interpreting geological carbon isotope excursions, with implications for the rate of carbon injection across the PETM. *Earth and Planetary Science Letters*, 435, 1-13.

Knoll AH. (1994) Proterozoic and Early Cambrian Protists - Evidence for Accelerating Evolutionary Tempo. *Proceedings of the National Academy of Sciences of the United States of America*, 91, 6743-6750. Doi 10.1073/Pnas.91.15.6743

Knoll AH. (2011) The Multiple Origins of Complex Multicellularity. *Annual Review of Earth and Planetary Sciences, Vol 39*, 39, 217-239. Doi 10.1146/Annurev.Earth.031208.100209

Knoll AH. (2014) Paleobiological perspectives on early eukaryotic evolution. *Cold Spring Harbor Perspectives in Biology*, 6. doi:10.1101/cshperspect.a016121

Knoll AH, and Follows MJ. (2016) A bottom-up perspective on ecosystem change in Mesozoic oceans. *Proceedings of the Royal Society of London. Series B: Biological Sciences*, 283. 10.1098/rspb.2016.1755

Knoll AH, Javaux EJ, Hewitt D, and Cohen P. (2006) Eukaryotic organisms in Proterozoic oceans. *Philosophical Transactions of the Royal Society B: Biological Sciences*, 361, 1023-1038. 10.1098/rstb.2006.1843

Kump L. (2008) The rise of atmospheric oxygen. *Nature*, 451, 277-278.

Laakso TA, and Schrag DP. (2014) Regulation of atmospheric oxygen during the Proterozoic. *Earth and Planetary Science Letters*, 388, 81-91.

Laakso TA, and Schrag DP. (2017) A theory of atmospheric oxygen. *Geobiology*, 15, 366-384.

Laakso TA, and Schrag DP. (2018) Limitations on limitation. *Global Biogeochemical Cycles*, 32, 486-496.

Lamb DM, Awramik SM, Chapman DJ, and Zhu S. (2009) Evidence for eukaryotic diversification in the ~1800 million-year-old Changzhougou Formation, North China. *Precambrian Research*, 173, 93-104. 10.1016/j.precamres.2009.05.005

Lenton TM, Daines SJ, and Mills BJW. (2018) COPSE reloaded: An improved model of biogeochemical cycling over Phanerozoic time. *Earth-Science Reviews*, 178, 1-28.

Lenton TM, and Watson AJ. (2004) Biotic enhancement of weathering, atmospheric oxygen and carbon dioxide in the Neoproterozoic. *Geophysical Research Letters*, 31, L05202.

Love GD, Grosjean E, Stalvies C, Fike DA, Grotzinger JP, Bradley AS, Kelly AE, Bhatia M, Meredith W, Snape CE and others. (2009) Fossil steroids record the appearance of Demospongiae during the Cryogenian period. *Nature*, 457, 718-721. 10.1038/nature07673

Lyons TW, Reinhard CT, Love GD, and Xiao S. (2012) Geobiology of the Proterozoic Eon. In: *Fundamentals of Geobiology*. edited by AH Knoll, DE Canfield and KO Konhausers, Blackwell Publishing Ltd., p 371-402.

Lyons TW, Reinhard CT, and Planavsky NJ. (2014) The rise of oxygen in Earth's early ocean and atmosphere. *Nature*, 506, 307-315.

Marsh R, Müller SA, Yool A, and Edwards NR. (2011) Incorporation of the C-GOLDSTEIN efficient climate model into the GENIE framework: "eb_go_gs" configurations of GENIE. *Geoscientific Model Development*, 4, 957-992.

Massana R. (2011) Eukaryotic picoplankton in surface oceans. *Annual Review of Microbiology*, 65, 91-110.

Meyer KM, Kump LR, and Ridgwell A. (2008) Biogeochemical controls on photic-zone euxinia during the end-Permian mass extinction. *Geology*, 36, 747-750. doi:10.1130/g24618a.1

Mills DB, Ward LM, Jones C, Sweeten B, Forth M, Treusch AH, and Canfield DE. (2014) Oxygen requirements of the earliest animals. *Proceedings of the National Academy of Sciences, USA*, 111, 4168-4172.

Møller EF. (2005) Sloppy feeding in marine copepods: prey-size-dependent production of dissolved organic carbon. *Journal of Plankton Research*, 27, 27-35.

Moloney CL, and Field JG. (1989) General allometric equations for rates of nutrient ingestion and respiration in plankton organisms. *Limnology and Oceanography*, 34, 1290-1299.

Moloney CL, and Field JG. (1991) The size-based dynamics of plankton food webs. I. A simulation model of carbon and nitrogen flows. *Journal of Plankton Research*, 13, 1003-1038.

Monteiro FM, Pancost RD, Ridgwell A, and Donnadieu Y. (2012) Nutrients as the dominant control on the spread of anoxia and euxinia across the Cenomanian-Turonian oceanic anoxic event (OAE2): Model-data comparison. *Paleoceanography*, 27, PA4209.

Moreno AR, and Martiny AC. (2018) Ecological stoichiometry of ocean plankton. *Annual Review of Marine Science*, 10, 43-69.

Olson JM. (2006) Photosynthesis in the Archean Era. *Photosynthesis Research*, 88, 109-117.

Olson SL, Reinhard CT, and Lyons TW. (2016) Limited role for methane in the mid-Proterozoic greenhouse. *Proceedings of the National Academy of Sciences, USA*, 113, 11447-11452.

Ozaki K, Reinhard CT, and Tajika E. (2019) A sluggish mid-Proterozoic biosphere and its effect on Earth's redox balance. *Geobiology*, 17, 3-11. 10.1111/gbi.12317

Panchuk K, Ridgwell A, and Kump LR. (2008) Sedimentary response to Paleocene-Eocene Thermal Maximum carbon release: A model-data comparison. *Geology*, 36, 315-318. 10.1130/g24474a.1

Pang K, Tang Q, Yuan XL, Wan B, and Xiao S. (2015) A biomechanical analysis of the early eukaryotic fossil Valeria and new occurrence of organic-walled microfossils from the Paleo-Mesoproterozoic Ruyang Group. *Paleoworld*, 24, 251-262.

Papineau D. (2010) Global biogeochemical changes at both ends of the Proterozoic: Insights from phosphorites. *Astrobiology*, 10, 165-181.

Parfrey LW, Lahr DJG, Knoll AH, and Katz LA. (2011) Estimating the timing of early eukaryotic diversification with multigene molecular clocks. *Proceedings of the National Academy of Sciences*, 108, 13624-13629. 10.1073/pnas.1110633108

Peng Y, Bao H, and Yuan X. (2009) New morphological observations for Paleoproterozoic acritarchs from the Chuanglinggou Formation, North China. *Precambrian Research*, 168, 223-232.

Planavsky N, Rouxel O, Bekker A, LaLonde SV, Konhauser KO, Reinhard CT, and Lyons TW. (2010) The evolution of the marine phosphate reservoir. *Nature*, 467, 1088–1090.

Planavsky NJ. (2015) The elements of marine life. *Nature Geoscience*, 7, 855-856.

Porter SM. (2016) Tiny vampires in ancient seas: evidence for predation via perforation in fossils from the 780-740 million-year-old Chuar Group, Grand Canyon, USA. *Proceedings of the Royal Society B*, 283. 10.1098/rspb.2016.0221

Porter SM, Agic H, and Riedman LA. (2018) Anoxic ecosystems and early eukaryotes. *Emerging Topics in Life Sciences*, 2, 299-309.

Porter SM, and Knoll AH. (2000) Testate amoebae in the Neoproterozoic Era: evidence from vase-shaped microfossils in the Chuar Group, Grand Canyon. *Paleobiology*, 26, 360-385. 10.1666/0094-8373(2000)026<0360:taitne>2.0.co;2

Porter SM, Meisterfeld R, and Knoll AH. (2003) Vase-shaped microfossils from the Neoproterozoic Chuar Group, Grand Canyon: A classification guided by modern testate amoebae. *Journal of Paleontology*, 77, 409-429.

Price NM, Ahner BA, and Morel FMM. (1994) The equatorial Pacific Ocean: Grazer-controlled phytoplankton populations in an iron-limited ecosystem. *Limnology and Oceanography*, 39, 520-534.

Reinhard CT, Planavsky NJ, Gill BC, Ozaki K, Robbins LJ, Lyons TW, Fischer WW, Wang C, Cole DB, and Konhauser KO. (2017) Evolution of the global phosphorus cycle. *Nature*, 541, 386-389.

Reinhard CT, Planavsky NJ, Olson SL, Lyons TW, and Erwin DH. (2016) Earth's oxygen cycle and the evolution of animal life. *Proceedings of the National Academy of Sciences, USA*, 113, 8933-8938.

Ridgwell A. (2007) Interpreting transient carbonate compensation depth changes by marine sediment core modeling. *Paleoceanography*, 22. 10.1029/2006pa001372

Ridgwell A, Hargreaves JC, Edwards NR, Annan JD, Lenton TM, Marsh R, Yool A, and Watson A. (2007) Marine geochemical data assimilation in an efficient Earth System Model of global biogeochemical cycling. *Biogeosciences*, 4, 87-104.

Ridgwell A, and Schmidt DN. (2010) Past constraints on the vulnerability of marine calcifiers to massive carbon dioxide release. *Nature Geoscience*, 3, 196-200.

Sanders RW. (1991) Mixotrophic protists in marine and freshwater ecosystems. *Journal of Eukaryotic Microbiology*, 38, 76-81.

Sperling EA, Halverson GP, Knoll AH, Macdonald FA, and Johnston DT. (2013) A basin redox transect at the dawn of animal life. *Earth and Planetary Science Letters*, 371-372, 143-155.

Sperling EA, and Stockey RG. (2018) The temporal and environmental context of early animal evolution: Considering all the ingredients of an "explosion". *Integrative and Comparative Biology*, 58, 605-622.

Stoecker DK, Hansen PJ, Caron DA, and Mitra A. (2017) Mixotrophyin the marine plankton. *Annual Review of Marine Science*, 9, 311-335.

Tittel J, Bissinger V, Zippel B, Gaedke U, Bell E, Lorke A, and Kamjunke N. (2003) Mixotrophs combine resource use to outcompete specialists: Implications for aquatic food webs. *Proceedings of the National Academy of Sciences, USA*, 100, 12776-12781.

Vallina SM, Ward BA, Dutkiewicz S, and Follows MJ. (2014) Maximal feeding with active prey-switching: A kill-the-winner functional response and its effect on global diversity and biogeography. *Progress in Oceanography*, 120, 93-109.

van Maldegem LM, Sansjofre P, Weijers JWH, Wolkenstein K, Strother PK, Wörmer L, Hefter J, Nettersheim BJ, Hoshino Y, Schouten S and others. (2019) Bisnorgammacerane traces predatory pressure and the persistent rise of algal ecosystems after Snowball Earth. *Nature Communications*, 10, 476.

Vidal G, and Moczydlowska-Vidal M. (1997) Biodiversity, speciation, and extinction trends of Proterozoic and Cambrian phytoplankton. *Paleobiology*, 23, 230-246.

Ward BA, Dutkiewicz S, and Follows MJ. (2014) Modelling spatial and temporal patterns in size-structured marine plankton communities: top-down and bottom-up controls. *Journal of Plankton Research*, 36, 31-47.

Ward BA, Dutkiewicz S, Jahn O, and Follows MJ. (2012) A size-structured food-web model for the global ocean. *Limnology and Oceanography*, 57, 1877-1891.

Ward BA, and Follows MJ. (2016) Marine mixotrophy increases trophic transfer efficiency, mean organism size, and vertical carbon flux. *Proceedings of the National Academy of Sciences, USA*, 113, 2958-2963.

Ward BA, Wilson JD, Death RM, Monteiro FM, Yool A, and Ridgwell A. (2018) EcoGEnIE 1.0: plankton ecology in the cGEnIE Earth system model. *Geoscientific Model Development*, 11, 4241-4267.

Wilson JD, Monteiro FM, Schmidt DN, Ward BA, and Ridgwell A. (2018) Linking marine plankton ecosystems and climate: A new modeling approach to the warm early Eocene climate. *Paleoceanography and Paleoclimatology*, 33, 1439-1452.

Xiao S, and Laflamme M. (2008) On the eve of animal radiation: phylogeny, ecology and evolution of the Ediacara biotia. *Trends in Ecology & Evolution*, 24, 31-40.

Xiong J, Fischer WM, Inoue K, Nakahara M, and Bauer CE. (2000) Molecular evidence for the early evolution of photosynthesis. *Science*, 289, 1724-1730.

Zumberge A, Love GD, Cárdenas P, Sperling EA, Gunasekera S, Rohrssen M, Grosjean E, Grotzinger JP, and Summons RE. (2018) Demosponge steroid biomarker 26-methylstigmastane provides evidence for Neoproterozoic animals. *Nature Ecology & Evolution*, 2, 1709-1714.

Zumberge JA, Rocher D, and Love GD. (In press) Free and kerogen-bound biomarkers from late Tonian sedimentary rocks record abundant eukaryotes in mid-Neoproterozoic marine communities. *Geobiology*. 10.1111/gbi.12378